# Mesh Size and Damped Edge Effects in Micromagnetic Spin Wave Simulations

G. Venkat, M. Franchin, H. Fangohr and A. Prabhakar



***Abstract*—We have studied the dependence of spin wave dispersion on the characteristics of the mesh used in a finite element micromagnetic simulation. It is shown that the dispersion curve has a cut off at a frequency which is analytically predictable. The frequency depends on the average mesh length used for the simulation. Based on this, a recipe to effectively obtain the dispersion relation has been suggested. In a separate study, spin wave reflections are absorbed by introducing highly damped edges in the device. However, an abrupt change in the damping parameter causes reflections. We compare damping profiles and identify an exponential damping profile as causing significantly less reflections.**

***Index Terms*—Computational micromagnetics, spin wave dispersion, absorbing boundary conditions**

## Introduction

In recent years, micromagnetic simulations have been used to investigate spin wave (SW) dynamics in ferromagnets [1], [2], and also obtain the spin wave dispersion of magnetic nanostructures [3]–[5]. While these simulations provide a convenient means of carrying out such investigations, proper care must be taken to guarantee the accuracy of the results obtained. We must also adjust the simulation parameters so as to better match experimental results. All this must be done keeping the computational resources, such as memory, available in mind.

We consider SW simulations, carried out for obtaining the SW dispersion of a ferromagnetic stripe, using the finite element micromagnetic package Nmag [6]. The problem considered was similar to the one described in [4]. There the aim of the simulation was to obtain the SW dispersion of the stripe and to compare it with analytic estimates. Further analysis revealed that the SW dispersion strongly depends on the mesh characteristics and the latter needs to be tailored for obtaining the desired dispersion. Here, we initially elaborate more on the computational aspects of the simulation. Schemes to decrease the computational complexity of finite element micromagnetic simulations have been studied [7], [8]. The dependency of the dispersion curves on the characteristics of the mesh used are detailed and an iterative scheme of designing the simulation, based on the computational resources available, is discussed.

In a separate study, we also consider the absorption of SW reflections by introducing highly damped edges at the end of the device. Periodic boundary conditions have been used to simulate SW propagation in permalloy films as well as magnonic crystals [9]–[11] while absorbing boundary conditions (ABCs) have been investigated before in spin torque simulations [12], [13]. We look at different damping profiles for absorbing SWs using finite element simulations. An exponentially damped profile seems to be optimum in reducing SW reflections from interfaces and edges.

G. Venkat and A. Prabhakar are with the Dept. of Electrical Engineering, Indian Institute of Technology – Madras, Chennai 600036, India (email: ee11d037@ee.iitm.ac.in)

M. Franchin and H. Fangohr are with Engineering and the Environment, University of Southampton, Southampton, SO17 1BJ, United Kingdom.

## Problem Specifications

We considered a stripe of permalloy ($Ni_{80}Fe_{20}$) having dimensions $600\times100\times5\,\text{nm}^3$ (Fig. 1) and material parameters given in Table I [14].

Table I
THE MATERIAL PARAMETERS OF PERMALLOY.

| Parameter | Value |
|---|---|
| Saturation Magnetization ($M_s$) | $8.6\times10^5$A/m |
| Exchange Constant ($A$) | $1.3\times10^{-11}$J/m |
| Anisotropy Constant ($K$) | 0 J/m$^3$ |
| Gyromagnetic ratio ($\gamma$) | $1.7\times10^{11}$Hz/T |

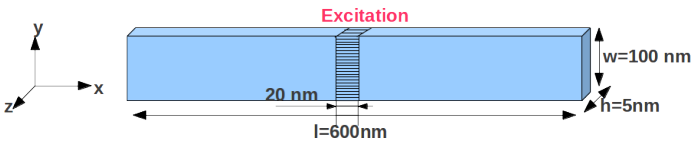


Figure 1. The geometry of the permalloy stripe being studied. The shaded region in the centre is where the SW excitation pulse is applied.

We are solving the normalized Landau-Lifshtiz equation [15], [16]

$$\frac{\partial \mathbf{m}}{\partial t} = -\gamma' \left[\mathbf{m}\times\mathbf{H} + \alpha\left(\mathbf{m}\times(\mathbf{m}\times\mathbf{H})\right)\right], \qquad (1)$$

where $\mathbf{m} = \mathbf{M}/M_S$ is the normalized magnetization with $\mathbf{M}$ and $\mathbf{H}$ being the total magnetization and effective field at any given time $t$, respectively. Here $\gamma' = \gamma\mu_0/(1+\alpha^2)$ with $\gamma$ being the electron gyromagnetic ratio ($\gamma<0$), $\alpha$ the phenomenological Gilbert damping and $\mu_0$ the permeability of free space. Although (1) is mathematically equivalent to the Landau-Lifshitz-Gilbert equation, where damping has the form $\mathbf{m}\times\frac{d\mathbf{m}}{dt}$, the physics for large values of $\alpha$ is different [17].

The damping ($\alpha$) was set to zero throughout, as is typical for a SW simulation [4]. The magnetization was initially saturated by applying a high bias magnetic field ($\mathbf{H}_0 = 804\,\text{kA/m}$) in a direction which decided the configuration of the spin waves namely backward volume (BV), forward volume (FV)

or surface wave [18]. A pulsed excitation magnetic field of the form

$$|\mathbf{h}|\,(t) = \Gamma\,\frac{\sin\left(2\pi f_{\text{exc}}\,(t-t_0)\right)}{2\pi f_{\text{exc}}\,(t-t_0)}, \tag{2}$$

with the excitation cutoff frequency $f_{\text{exc}} = 200\,\text{GHz}$, $t_0 = 50\,\text{ps}$, and amplitude $\Gamma = 400\,\text{kA/m}$, was applied in a small region in the centre. Since this pulse is rectangular in the Fourier domain, this ensured that all frequencies in a band are uniformly excited. The high value of $\Gamma$ ensured that the modes excited had sufficient amplitude while the the offset $t_0$ ensured that the excitation did not have spurious high frequency components.

SW dispersion curves for this problem, obtained using the micromagnetic solver OOMMF [19] have been described elsewhere [4]. A dispersion curve is obtained by viewing a surface plot of the Fourier transform of a component of the magnetization e.g. $m_y\,(k_x, \omega)$. This is defined by [3], [4]

$$m_y\,(k_x, \omega) = \left|\mathcal{F}_2\left[m_y\,(x, y_0, z_0, t) - m_y\,(x, y_0, z_0, 0)\right]\right|, \tag{3}$$

where $\mathcal{F}_2$ is the 2-D Fourier transform operator and $y_0$ and $z_0$ are at the centre of the stripe. We used a temporal resolution of 1 ps and a spatial resolution of 1 nm which ensured that Nyquist's sampling theorem is satisfied and aliasing does not occur. A Hanning window function

$$H\,(n) = \frac{1}{2}\left[1 - \cos\left(\frac{2\pi n}{N-1}\right)\right], \quad 0 \le n \le N-1, \tag{4}$$

where $N$ is the number of samples, was applied in time and space, to reduce the artifacts caused by having finite number of samples [5].

We start off by showing the magnitude of the spectrum defined by (3) (in a dB scale), in which typical dispersion curves for volume and surface SW configurations are visible (Fig. 2).

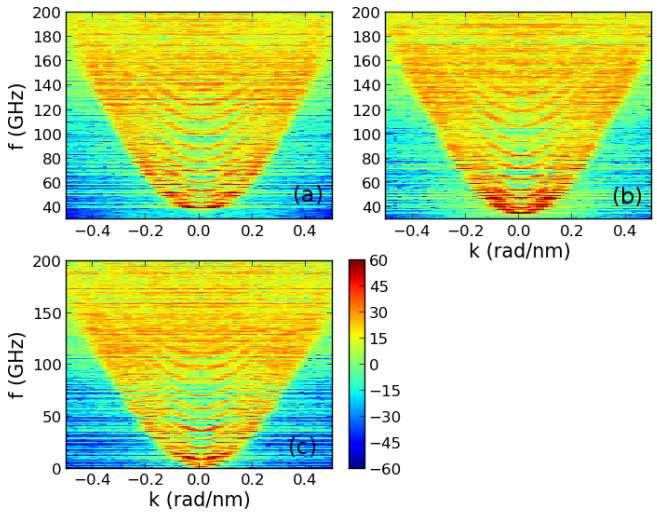


Figure 2. The magnitude of the magnetization spectrum (in a dB scale) showing the dispersion curves of SWs in (a) BV, (b) surface wave and (c) FV configurations.

The different curves, in each plot, correspond to the quantized modes along the width of the stripe. The absence of the band gap below $\approx 40\,\text{GHz}$, in the FV configuration, is because the demagnetization field is $H_{\text{demag}} = -M_{\text{s}}$ [4]. The fundamental (lowest order) mode contains more power (more red) than the other modes. The dispersion curves are parabolic because the SWs are exchange dominated [20].

The mesh used in a finite element simulation plays a prominent role in determining the quality of results obtained. In a typical micromagnetic simulation, the average mesh length ($l_{\text{av}}$) is chosen to be less than the exchange length ($l_{\text{ex}}$) (which is the interaction with the smallest length scale). For a material with no significant crystalline anisotropy, like permalloy,

$$l_{\text{ex}} = \sqrt{\frac{2A}{\mu_0 M_{\text{s}}^2}} \approx 5.7\,\text{nm} \tag{5}$$

using the values given in Table I. A histogram of the elements of a tetrahedral mesh, generated by the package Gmsh [21], is shown in Fig. 3 along with a snapshot of the mesh. The corners of the stripe will have elements of smaller edge lengths while elements near the centre have large edge lengths.

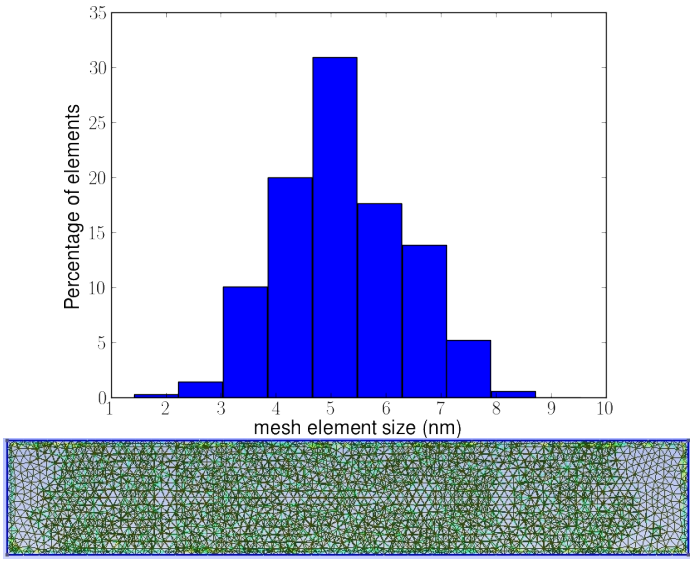


Figure 3. A histogram of the mesh element size (top) and an image of the mesh (bottom).

The mesh had 20681 volume elements, 12950 surface elements and $l_{\text{av}} = 5.17\,\text{nm}$. The number of surface nodes (which increases with decrease in mesh size) was $n_{\text{SN}} = 6477$. In order to solve the LLG equation, Nmag creates a boundary element matrix (BEM) of the points in the mesh. The BEM size is given by

$$S_{\text{BEM}} \sim n_{\text{SN}}^2 \times 8\,\text{bytes}. \tag{6}$$

These mesh statistics correspond to a BEM of size 320 MB which is quite large for such a small structure. Thus it can be seen that decreasing the mesh size can make computational costs prohibitive.

## MESH EFFECTS ON SW DISPERSION

We considered three different meshes for a comparative study of the mesh characteristics on the spin wave dispersion. Since the stripe is saturated, we do not have any domain walls

or vortices in the stripe. The meshes used were created using Gmsh and had $l_{\text{av}}$ values of 5.2, 6.2 and 9.2 nm. Fig. 4 shows the dispersion curves, obtained using these different meshes, for the BVSW configuration.

Although the excitation pulse allows for modes till $f_{\text{exc}} = 200$ GHz, each plot exhibits a cutoff frequency (shown by black dotted lines). Moreover this cutoff frequency clearly depends on the value of $l_{\text{av}}$ for the mesh. The modes above the cutoff frequency are not clear in all the dispersion curves obtained using the Gmsh meshes.

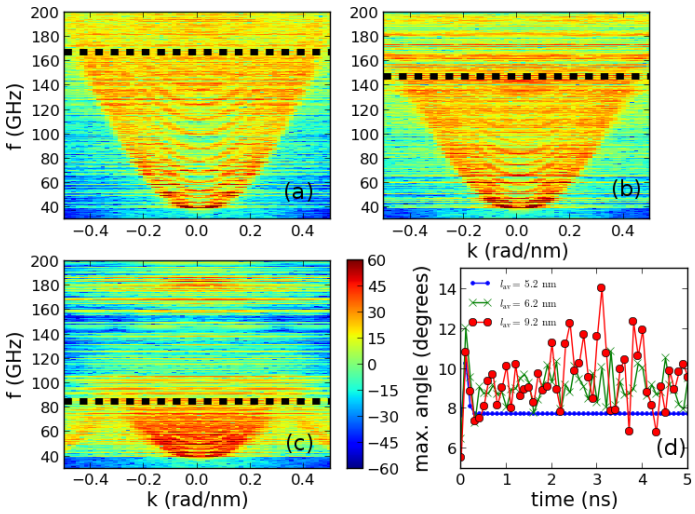


Figure 4. The magnetiude of magnetization spectrum (in a dB scale) showing the dispersion curves along the stripe obtained from meshes with average mesh size (a) 5.2, (b) 6.2 and (c) 9.2 nm created using Gmsh. The dotted lines mark the cutoff frequencies. (d) shows the variation of the maximum angle of the change in magnetization from one node to the next in the mesh with simulation duration.

It is worthwhile to monitor the maximum angle of the change in magnetization from one node to the next in the mesh. The results are probably reliable if this angle is less than 30° throughout the simulation [22]. Fig. 4 (d) shows this quantity for half the simulation duration. We can see that with a fine mesh ($l_{\text{av}} = 5.2$ nm) the angle approaches steady state after an initial peak while this is not the case with the rougher meshes. However in all the cases, the maximum angle is well below 30°.

The dispersion relations for the lowest order exchange dominated spin wave mode, for volume and surface SW configurations, are given by

$$\omega^2 = \begin{cases} \omega_{\text{ex}}.\left(\omega_{\text{ex}} + \omega_{\text{M}}\frac{1-e^{-kh}}{kh}\right) & \text{BV} \\ \omega_{\text{ex}}.\left(\omega_{\text{ex}} + \omega_{\text{M}}\left(1 - \frac{1-e^{-kh}}{kh}\right)\right) & \text{FV} \\ \omega_{\text{ex}}.\left(\omega_{\text{ex}} + \omega_{\text{M}}\right) + \frac{\omega_{\text{M}}^2}{4}\left(1 - e^{-2kh}\right) & \text{Surface} \end{cases} \quad (7)$$

where we have included exchange interaction in the expressions derived by Kalinikos for dipolar spin waves [23]. Here

$$\omega_{\text{ex}} = \omega_0 + \lambda_{\text{ex}}\omega_{\text{M}}k^2, \quad (8)$$

$\omega$ is the frequency of oscillation of the spin wave with wave vector $\mathbf{k}$, $\omega_0 = \gamma\mu_0|\mathbf{H}_0|$ is the uniform precession mode frequency, $\omega_{\text{M}} = \gamma\mu_0 M_{\text{s}}$, $\lambda_{\text{ex}} = (l_{\text{ex}})^2$ is the phenomenological exchange constant, the thickness $h = 5$ nm and $k = |\mathbf{k}|$. Let us, for the moment, consider the BV configuration. In the large $k$ limit, the dispersion relation reduces to

$$\omega = \omega_{\text{ex}} = \omega_0 + \omega_M\lambda_{\text{ex}}k^2. \quad (9)$$

From (8), we expect a finite element simulation to yield good dispersion curves up to a cut-off frequency $\omega_{\text{c}}$, and we also expect $\omega_c$ to have a linear dependence on $k^2$. The values of $\omega_{\text{c}}$ were read off the first three dispersion curves in Fig. 4 and indeed in Fig. 5, we observe that $\omega_c \propto l_{\text{av}}^{-2}$ (where $k \propto l_{\text{av}}^{-1}$). The errorbars show the deviation of the values obtained from the analysis pertaining to (9) from the values read off from the dispersion curves in Fig. 4. Fig. 5 also shows that this analysis holds true for FV and surface SW configurations.

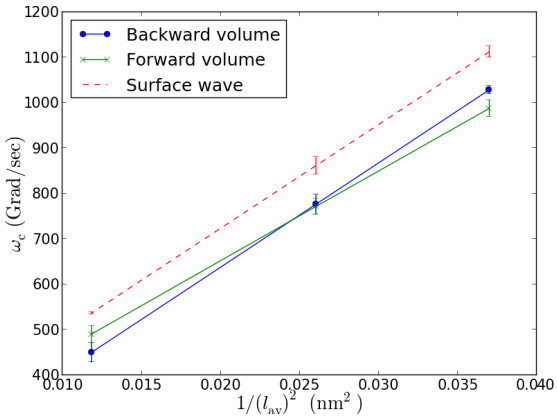


Figure 5. Dependence of the cut-off frequency on the average finite element edge length, for the different spin wave configurations.

Rewriting (9), we obtain and estimate the average finite element length as

$$l_{\text{av}} \propto \sqrt{\frac{2A\gamma}{M_{\text{s}}\left(\omega_{\text{c}} - \gamma\mu_0 H_0\right)}}. \quad (10)$$

We are now in a position to propose a recipe suitable for obtaining the reliable dispersion relation $\omega(k)$ from finite element simulations.

- Decide what $\omega_{\text{c}}$ is suitable for the application in mind.
- Use (9) to find $k_{\text{c}}$ and subsequently $l_{\text{av}}$ from (10).
- Choose a sampling in time and space as $\Delta t = \frac{\pi}{\omega_{\text{c}}}$ and $\Delta x = \frac{\pi}{k}$, respectively, to satisfy Nyquist's criterion while evaluating (3).
- Choose a cutoff frequency for the excitation signal in (2) as $f_{\text{exc}} = \frac{1}{2\pi}\omega_{\text{c}}$
- Apply the Hanning window (4), on the time-space data, before computing the dispersion
- This procedure may need to be repeated for obtaining the optimum dispersion curve.

## Damped edges that absorb reflections

When we seek to model realistic magnonic devices but use finite size geometries, we often face the problem of reflections off the edges of the device. A typical example would be a magnonic ring with stubs [24]. In an experiment reflections are avoided by using a sufficiently long length for the stubs. However, the computational overhead could be significant in

a finite element micromagnetic simulation. In such cases we introduce artificial regions of high Gilbert damping [25] at the edges of the device.

There are two approaches that have been proposed for this purpose. The initial method proposed was to have a gradual change in damping so as to reduce reflections from the undamped - damped regions interface [12]. Later on an abrupt change in damping was proposed [13] which seemed to perform satisfactorily without an unmanageable increase in the computational expense. We tried both the approaches in order to find the most efficient method for absorbing the reflections.

The problem was modified to the following:

- The stripe had a damped edge at one of the ends (shown in Fig. 6).

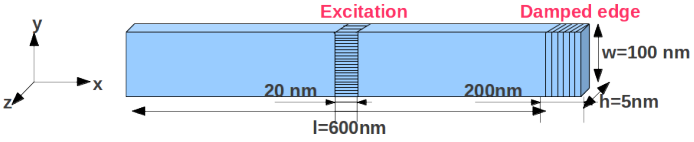


Figure 6. The geometry of the simulation with damped edges.

- Three different damping profiles (Fig. 7) considered were
  - constant
  - piecewise constant and
  - exponential (The exponential profile parameters shown were chosen so that there is no discontinuity in $\alpha$ at the damped - undamped interface.).

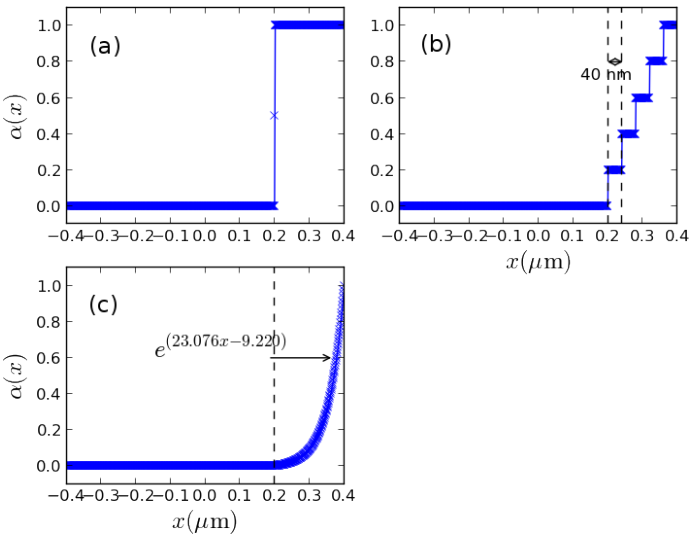


Figure 7. The damping profiles considered are (a) constant (b) piecewise constant and (c) exponential.

- The propagation of a narrow pulse was to be observed along the stripe. Accordingly, some of the parameters of the excitation pulse were changed to $f_{exc} = 100\,\text{GHz}$, $t_0 = 5\,\text{ps}$. The pulse was applied for $10\,\text{ps}$.

In finite difference time domain (FDTD) simulations, a perfectly matched layer (PML) is an efficient method to terminate a grid [26]. In the PML, the spatial variation of the conductivity (or loss) is taken as [27]

$$\sigma(z) = \sigma_m \left(\frac{z}{d}\right)^n, \tag{11}$$

where $z$ is the depth within the PML region of total depth $d$. The order of the conductivity profile ($n$) needs to be optimized to efficiently absorb the waves at the edges. Too low an exponent will lead to a bad fit, while too high a value will lead to many spurious oscillations in the wave absorbing region. We found that our exponential profile fits well to a polynomial of the form

$$\alpha_{fit}(x) = 0.0026 \left(\frac{x}{L}\right)^{8.6}, \tag{12}$$

where $x$ is in nm and $L = 200\,\text{nm}$ is the length of the SW damping region. The polynomial order is close to the range of values obtained by performing a multiobjective algorithm analysis for a PML in FDTD simulations [27].

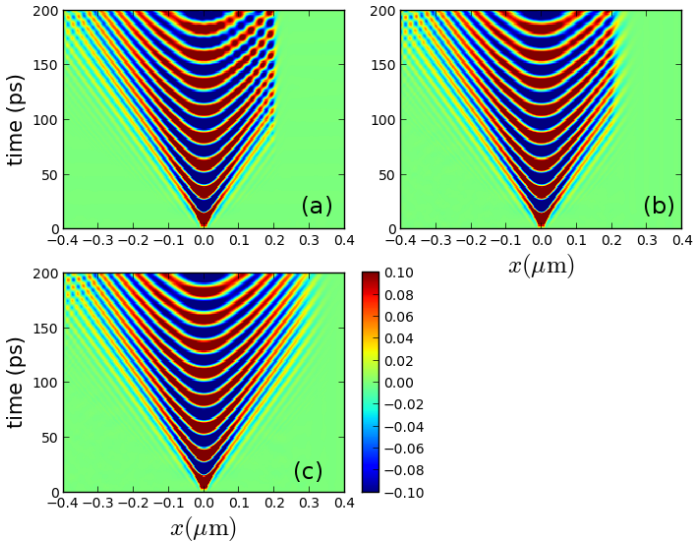


Figure 8. Spatio-temporal evolution of spin wave amplitude after excitation at $x = 0$, $t = 0$. The right edge of the stripe has (a) constant, (b) piecewise constant and (c) exponentially damped profiles shown in Fig. 7.

Fig. 8 helps visualize the effects of the different forms of damping. We observe that the reflections from the damped - undamped interface is most pronounced in Fig. 8(a) and the least in Fig. 8(c). The effects of reflections from the left edge (having no damped edge) is prominent in all the plots. On the other hand, waves approaching the damped edge (at $x = 0.2\,\mu\text{m}$) in Fig. 8(c) seem to be relatively unchanged indicating that reflections from the device edge are absorbed in the damped edge. Thus the exponential increase in $\alpha$ appears to be very efficient, in terms of minimizing reflections from both the damped - undamped interface and the device edge. An alternate approach would be to use a spatially non-uniform magnetic field at the edges, as suggested by early experiments on YIG [28].

It is necessary to determine the length of the damped region required to sufficiently attenuate the reflections occurring from the edges of the device. After extracting $m_y(x,t)$ from the simulation data, we calculated the energy

$$\mathcal{E}(x) = \int_{T_{start}}^{T_{stop}} |m_y(x,t)|^2 dt, \tag{13}$$

using the trapezoidal rule. We took $T_{\text{start}} = 1\,\text{ns}$ to leave out any transient effects caused by the excitation pulse. The spatial damping rates, for the different damping profiles, are shown in Fig. 9. Note that that the damping coefficient of the amplitude ($m_y(x)$) will be half of these damping coefficients (due to squaring in (11)).

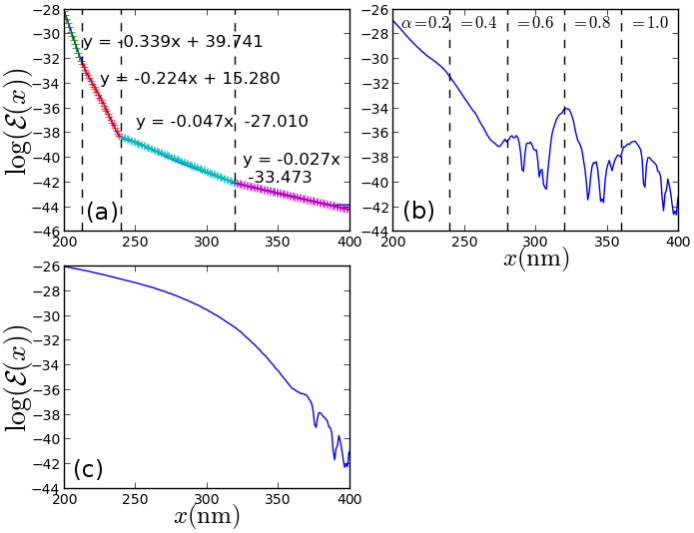


Figure 9. The propagation of the spin waves in the damped region as a function of length in the (a) constant (b) piecewise constant and (c) exponentially damped edge.

In the constantly damped profile, there is a non uniform logarithmic decrease in different parts of the damped edge. The different spatial damping rates have been extracted for different regions and are shown in Fig. 9(a). In the piecewise constant damped profile, there is an exponential decrease till around $x < 280\,\text{nm}$. In the exponentially damped profile, there is a far more gradual decrease in the spin wave amplitude.

It is instructive to validate the amplitude decay rate of $2|\alpha_x| = 0.027\,\text{nm}^{-1}$ obtained from the last fit for $x > 320\,\text{nm}$ in Fig. 9(a), against an apriori specified parameter. We consider the parameters in (1). Using simple dimensional analysis, we can see that

$$2\pi \times \alpha_x \times v_\text{g} = \alpha \times \gamma\mu_0 H_0 \tag{14}$$

where both sides have units of cyclic frequency ($\omega$) i.e. rad/s. Using $H_0 = 8 \times 10^5\,\text{A/m}$ and $v_g = 2000\,\text{m/s}$, we obtain

$$\alpha = \alpha_x v_\text{g} f_0^{-1} \approx 1, \tag{15}$$

where $2\pi f_0 = \gamma\mu_0 H_0 = 2\pi(28.27\,\text{GHz})$ is at the bottom of the spin wave band. This is consistent with the value of $\alpha$ specified in the abruptly damped edge. The group velocity $v_\text{g}$ was estimated from the plots in Fig. 8, which show the spin wave amplitude after being excited at the centre of the stripe. We thus infer that the higher damping rates seen for $200 < x < 320\,\text{nm}$ are caused by the abrupt introduction of damping, and it takes approximately $120\,\text{nm}$ to reach steady state due to the low value of $v_\text{g}$ of BV waves.

## Summary

Good simulations help us develop an intuition for a physical problem. In a finite element simulation, the mesh plays a crucial part in producing correct results. In finite element micromagnetic simulations, spin wave dispersion shows a cut off at a frequency which depends on the average edge length in the mesh that we use. Based on our observations,, we propose a recipe for the effective mesh size to obtain dispersion curves.

Reducing unwanted reflections from the boundaries is important for accurate simulations of magnonic devices. While these reflections are easily avoided in experiments by creating longer stubs, larger devices would place an unnecessary burden on the computational resources. Abrupt changes in damping can also cause spurious artifacts. By introducing an exponential increase in damping, we were able to suppress the reflections from the damped-undamped interface.

## References


[1] S.-K. Kim, "Micromagnetic computer simulations of spin waves in nanometre-scale patterned magnetic elements," *J. Phys. D: App. Phys.*, vol. 43, p. 264004, 2010.

[2] S. Bance *et al.*, "Micromagnetic calculation of spin wave propagation for magnetologic devices," *J. Appl. Phys.*, vol. 103, p. 07E735, 2008.

[3] V. Kruglyak and R. Hicken, "Magnonics: Experiment to prove the concept," *J. Magn. Magn. Mater.*, vol. 306, p. 191, 2006.

[4] G. Venkat *et al.*, "Proposal for a standard micromagnetic problem: Spin wave dispersion in a magnonic waveguide," *IEEE Trans. Magn.*, vol. 49, p. 524, 2013.

[5] D. Kumar *et al.*, "Numerical calculation of spin wave dispersions in magnetic nanostructures," *J. Phys. D: Appl. Phys.*, vol. 45, p. 015001, 2012.

[6] T. Fischbacher *et al.*, "A systematic approach to multiphysics extensions of finite-element-based micromagnetic simulations: Nmag," *IEEE Trans. Magn.*, vol. 43, p. 2896, 2007.

[7] K. Ramstock, T. Leibl, and A. Hubert, "Optimizing stray field computations in finite-element micromagnetics," *Journal of Magnetism and Magnetic Materials*, vol. 135, pp. 97 – 110, 1994.

[8] A. Kakay, E. Westphal, and R. Hertel, "Speedup of fem micromagnetic simulations with graphical processing units," *Magnetics, IEEE Transactions on*, vol. 46, pp. 2303–2306, 2010.

[9] L. Fallarino *et al.*, "Propagation of spin waves excited in a permalloy film by a finite-ground coplanar waveguide: A combined phase-sensitive micro-focused brillouin light scattering and micromagnetic study," *IEEE Trans. Magn.*, vol. 49, pp. 1033–1036, 2013.

[10] J. Yoon, C.-Y. You, and M.-H. Jung, "Dynamic susceptibility of thin films with perpendicular magnetic anisotropy," *Current Applied Physics*, vol. 13, pp. 1765 – 1768, 2013.

[11] O. Dmytriiev, V. V. Kruglyak, M. Franchin, H. Fangohr, L. Giovannini, and F. Montoncello, "Role of boundaries in micromagnetic calculations of magnonic spectra of arrays of magnetic nanoelements," *Phys. Rev. B*, vol. 87, p. 174422, May 2013.

[12] D. V. Berkov and N. L. Gorn, "Micromagnetic simulations of the magnetization precession induced by a spin-polarized current in a point-contact geometry (invited)," *J. Appl. Phys.*, vol. 99, p. 08Q701, 2006.

[13] G. Consolo *et al.*, "Boundary conditions for spin-wave absorption based on different site-dependent damping functions," *IEEE Trans. Magn.*, vol. 43, p. 2974, 2007.

[14] A. Hubert and R. Schafer, *Magnetic Domains: The Analysis of Magnetic Microstructures*. Berlin: Springer, 1998.

[15] L. Landau and L. Lifshitz, *Phys. Zeit. Sowjetunion*, vol. 8, p. 153, 1935.

[16] M. Franchin, Ph.D. dissertation, Univ. of Southampton, 2009.

[17] J. Mallinson, "On damped gyromagnetic precession," *IEEE Trans. Magn.*, vol. 23, pp. 2003 – 2004, 1987.

[18] D. D. Stancil and A. Prabhakar, *Spin Waves Theory and Applications*, 1st ed. New York: Springer, 2008.

[19] M. Donahue and D. Porter, "OOMMF user's guide, version 1.0," National Institute of Standards and Technology, Gaithersburg, MD, Tech. Rep., 1999. [Online]. Available: http://math.nist.gov/oommf/

[20] C. Kittel, *Introduction to Solid State Physics*, 8th ed. New York: John Wiley and Sons, 2010.

[21] C. Geuzaine and J. Remacle, "Gmsh: A 3-d finite element mesh generator with built-in pre- and post-processing facilities," *Int. J. Numer. Meth. Eng.*, vol. 79, p. 1309, 2009.

[22] H. Fangohr *et al.*, "NMAG user manual (0.2.1)," University of Southampton, Tech. Rep., 2012. [Online]. Available: http://nmag.soton.ac.uk/nmag/0.2/manual/html/manual.html
[23] B. Kalinikos, "Excitation of propagating spin waves in ferromagnetic films," *IEE Proc.*, vol. 127, p. 4, 1980.
[24] G. Venkat *et al.*, "Spin wave propagation in permalloy rings." Intl. Conf. Microwave Magnetics, Kaiserslautern, Germany, 2012.
[25] T. Gilbert, "A phenomenological theory of damping in ferromagnetic materials," *IEEE Trans. Magn.*, vol. 40, p. 3443, 2004.
[26] J.-P. Berenger, "A perfectly matched layer for the absorption of electromagnetic waves," *J. Comput. Phys.*, vol. 114, pp. 185 – 200, 1994.
[27] X. L. Travassos, Jr. *et al.*, "Optimal configurations for perfectly matched layers in fdtd simulations," *IEEE Trans. Magn.*, vol. 42, pp. 563–566, 2006.
[28] S. J. Wallin and D. D. Stancil, "Suppression of magnetostatic backward volume wave end reflections via field gradients," *J. App. Phys.*, vol. 57, p. 3718, 1985.